Modeling Multi-Step Organic Reactions: Can Density Functional Theory Deliver Misleading Chemistry?

Hanwei Li, Maryam Mansoori Kermani, Alistar Ottochian, Orlando Crescenzi, Benjamin Janesko, Donald Truhlar, Giovanni Scalmani, Michael Frisch, Ilaria Ciofini, Carlo Adamo

Modeling Multi-Step Organic Reactions: Can Density Functional Theory Deliver Misleading Chemistry?

Hanwei Li[a,†], Maryam Mansoori Kermani[b,†], Alistar Ottochian[a], Orlando Crescenzi[c], Benjamin G. Janesko[d], Donald G. Truhlar[b,*], Giovanni Scalmani[e], Michael J. Frisch[e], Ilaria Ciofini[a], and Carlo Adamo[a,f,*]

a) *Chimie ParisTech, PSL Research University, CNRS, Institute of Chemistry for Life and Health Sciences, F-75005 Paris, France*
b) *Department of Chemistry, Chemical Theory Center, and Minnesota Supercomputing Institute, University of Minnesota, Minneapolis, MN 55455-0431, USA*
c) *Dipartimento di Scienze Chimiche, Università di Napoli Federico II, Complesso Universitario di Monte Sant'Angelo, Via Cinthia, 80126 Napoli, Italy*
d) *Department of Chemistry & Biochemistry, Texas Christian University, Fort Worth, TX 76129, USA*
e) *Gaussian, Inc.; Wallingford, CT 06492, USA*
f) *Institut Universitaire de France, 103 Boulevard Saint Michel, F-75005 Paris, France*

[†]These authors contributed equally.
*email: truhlar@umn.edu, carlo.adamo@chimieparistech.psl.eu

Abstract. Many organic reactions are characterized by a complex mechanism with a variety of transition states and intermediates of different chemical natures. Their correct and accurate theoretical characterization critically depends on the accuracy of the computational method used. In this work we study a complex ambimodal cycloaddition with five transition states, two intermediates, and three products, and we ask whether density functional theory (DFT) can provide a correct description of this type of complex and multifaceted reaction. Our work fills a gap in that most systematic benchmarks of DFT for chemical reactions have considered much simpler reactions. Our results show that many density functionals not only lead to seriously large errors but also differ from one another in predicting whether the reaction is ambimodal. Only a few of the available functionals provide a balanced description of the complex and multifaceted reactions. The parameters varied in the tested functionals are ingredients, the treatment of medium-range and nonlocal correlation energy, and the inclusion of Hartree-Fock exchange. These results show a clear need for more benchmarks on the mechanisms of large molecules in complex reactions.

Introduction.

Understanding the reaction mechanisms behind complex chemical transformations is a challenging issue at the heart of chemistry. One way to accomplish this is to propose reasonable reaction paths and try to discriminate among them by comparison of energetic and dynamical calculations to experimental data. In this context, computational insights obtained using quantum-chemical approaches have increasingly been combined with experimental data to support the feasibility of a reaction mechanism even for complex chemical phenomena (see refs 1 to 3 for examples). In some cases, though, one needs to assign mechanisms without having enough experimental data, and the reliability of this approach depends on knowing which, if any, theoretical methods can predict reaction paths with high enough energetic precision for the results to be trustworthy. To ascertain this, many tests have been carried out for various theoretical methods, but these tests are usually for simple reactions of small molecules. The question addressed here is how well one can trust the computational predictions for complex reaction paths of large organic molecules.

For this study, we have chosen the reactions that occur in the multistep mechanism for the cycloaddition of cycloheptatriene (**7**) to tropone (**1**), 2-chlorotropone (**1a**), and 2-methoxytropone (**1b**).[4–7] The mechanism of these reactions has been predicted by Jamieson et al.;[6,7] and their predicted energetics for structures along the reaction path for the unsubstituted case are shown in Figure 1; the figure shows energies for the reactants, five transition states, two intermediates, and three products. Structures **9**, **8**, **12**, and **11** all have one carbon-oxygen double bond; structures **8** and **9** have four carbon-carbon double bonds, while **12** and **11** have only two carbon-carbon double bonds. This difference in the number of double bonds suggests a different degree of electronic delocalization in the intermediates.

The reaction under study is ambimodal. Ambimodal reactions are reactions with a bifurcation (or trifurcation) of the reaction path after the highest free-energy-of-activation point on the reaction path (a bifurcation of a reaction path is often called a valley–ridge inflection point).[8–38] The products formed at the ends at the split reaction path may be different, and such reactions are very challenging for theoretical analysis because small differences in the relative barrier heights of the various stationary points can have a large effect on the product ratios and can also be determinative of whether the reaction is indeed ambimodal.

The reaction in Figure 1 is a [6+4] cycloaddition passing through tripericyclic transition state **TS5** to produce the intermediates **8** and **9**. Intermediate **9** can react by a [3,3]-sigmatropic Claisen rearrangement through **TS7** to produce the [8+2] cycloaddition product **10**, but **10** is a minor product because the transition state **TS7** is 3 kcal higher in energy than **TS5**. (All energies in this article are

molar energies.) The intermediates **8** and **9** undergo intramolecular Diels-Alder reactions through **TS8** and **TS9** to form products **11** and **12**, respectively. **TS8** is lower than **TS9** because the dienophile **8** is an activated α,β-unsaturated ketone. In addition, **8** and **9** can interconvert through Cope transition state **TS6**; however, **TS6** is higher in energy than either **TS8** or **TS9** so one might have expected **8** and **9** to interconvert more slowly than they evolve to their respective products. In summary, if the reaction course is dominated by these energetic considerations rather than by entropic effects and dynamics, one would expect the major product to be **11**, which is pentacyclic with 4-, 5-, 6-, and 7-membered rings. However, the four transition states are close in energy, and these conclusions depend on getting their relative energies correct or at least in the correct order. This is especially important because the product was found to be **11** in an experimental study of the reaction of the unsubstituted tropone, and the 7-chloro-**11** product was found for reaction of 2-chlorotropone, but another ring structure was found experimentally for reaction of 2-methoxytropone,[4] whereas Jamieson et al.'s computations showed the same mechanism for the unsubstituted and both substituted cases. However, the product ratios are not necessarily determined by the energetics, especially because these reactions are ambimodal with **TS5** higher than **TS6**, **TS8**, and **TS9**. Thus, trajectories started at **TS5** were found to produce all three products (**8**, **9**, and **10**).[6]

To explore this reaction or other complex reactions by trajectories or transition state theory, it is necessary to employ an accurate potential energy surface, and dynamics calculations are most affordable with density functional theory, so it is important to know if this theory gives accurate potential energies for all steps in the mechanism. Jamieson et al.[6,7] calculated the energetics by a high-level method, DLPNO-CCSD(T)/cc-pVQZ//ωB97X-D/def2-TZVP, and our previous study[39] of **TS8** and **TS9** at a more complete level indicated that this is accurate within about 0.5±1.0 kcal. Therefore, we use these previous energetics calculations as benchmarks, and we explore the accuracy of many density functional approximations.

The present study is relevant not just because of the importance of cycloaddition reactions, which are ubiquitous in synthesis and biochemisty,[6] but even more significantly because it differs from the great majority of previous tests of density functionals in that it considers a multistep reaction with bifurcating reaction paths and with intermediates and products having much more complex stereochemistry. The reactions considered in standard benchmarks are simple one-step reactions, characterized by the energy difference between reactant(s) and product(s) and one (forward) or two (forward and reverse) barriers. The present study is an attempt to answer the broad question: Can density functional theory (DFT) give accurate potential energies for multi-step organic reactions with crowded transition states, and if so, which density functional approximations

are most reliable? The density functionals considered in this work are presented with references[40–82] in Table 1.

The mechanism in Figure 1 is challenging because it contains three kinds of reaction. The step from **9** to **8** is a Cope rearrangement, that from **9** to **10** a Claisen rearrangement, and the products **12** and **11** are obtained via Diels-Alder reactions. Density functional approximations have been benchmarked for these types of reactions. The energies of the Cope rearrangements (barriers and reaction energies) are expected[83] to be predicted with a good accuracy (errors of 1–2 kcal) by PBE-QIDH, which is a doubly hybrid functional, and by several global hybrid functionals, such as ωB97X-V and M06-2X. In contrast, the doubly hybrid functionals B2PLYP and DSD-PBEP86 and the global hybrid functionals PBE0, M11 and B3LYP are expected to provide larger errors (greater than 4 kcal) on this type of reactions. Comparisons to benchmark data for Diels-Alder reactions indicate that the reaction energies are reproduced by DSD-PBEP86, M06-2X, PBE-QIDH, and M11plus with errors of ~2 kcal or less, while ωB97X-V, PBE-QIDH and M11 have errors of about 3 to 5 kcal[83–85]. In further contrast, energy barriers for pericyclic reactions are expected to be reproduced by DSD-PBEP86, B2PLYP, PBE-QIDH, M06-2X, and ωB97X-V with errors less than 2 kcal, while errors larger than 2 kcal are expected for ωB97X-V and M11[86,87]. Overall, these previous studies make it clear that even a qualitatively reliable description of the entire mechanism of Figure 1 by a single method represents a hard challenge for DFT.

In a recent study[39], we have focused on a small part of this reaction mechanism, namely the Diels-Alder reactions from **9** through **TS9** to **12** and from **8** through **TS8** to **11**, and we considered the energy of **TS8** and **TS9** relative to that of **1**+**7** and the energy of **TS9** relative to **TS8**. We found that only a few of the tested functionals, namely ωB97M-V, M11plus, ωB97X-V, PBE-D3, M11 and MN15, provide mean deviations from reference data that are less than 3.0 kcal. A perhaps surprising result is that the accurate functionals are of many different types and other functionals of those same types performed less well. This work showed that the energy of crowded and strained transition states is problematic for many density functionals and that the accuracy cannot be anticipated from the type of functional. Another unexpected result is that, despite huge differences in transition state energies relative to **1**+**7**, all the considered functionals predict **TS9** to be higher in energy than **TS8**.

Here we enlarge the investigation by analyzing the whole mechanism of Figure 1 for the cycloaddition of **7** to **1**, **1a**, and **1b**. We will first try to show how various density functional approximations differently affect the energetics of competitive reaction channels, due to unequal errors in the predicted kinetics (energy barriers) and thermochemistry (energy differences). Next,

we will explain and qualitatively correlate the computed behaviors to known shortcomings that, by construction, affect differently the exchange-correlation functionals used.

Before discussing our results, we consider the expected reliability of the benchmarks. The benchmark is based on DLPNO-CCSD(T)[88] calculations. DLPNO-CCSD(T) is a way to carry out CCSD(T) calculations[89] for large molecules. We have two concerns in estimating the reliability of DLPNO-CCSD(T): (1) the reliability of CCSD(T) itself; (2) the agreement of DLPNO-CCSD(T) with CCSD(T). The CCSD(T) method is well known to be more reliable for so-called singe-reference systems than for multireference systems.[90] Multireference character is a measure of the inherent multiconfiguration nature of a species and is associated with high static correlation, which is also called strong correlation. The simplest measure of multireference character is the B_1 diagnostic[91] or the generalized B_1 (GB1) diagnostic.[92] The B_1 diagnostic was originally introduced for ascertaining the multireference character in a bond.[91] As an extension, the GB1 diagnostic provides an indication of the change in multireference character in a reaction. For a chemical reaction, the GB1 diagnostic is the absolute value of the difference between the classical reaction energy or classical barrier height calculated with the BLYP density functional and the same quantity calculated with the B1LYP density functional. As a rough guide to multireference character, we established a guideline that 10 kcal is the boundary of severe multireference character.[67,91,92] In our previous work[39] we estimated the reliability of DLPNO-CCSD(T) as 0.5±1.0 kcal for **TS8** and **TS9** of the unsubstituted tropone reaction; these transition states have a GB1 diagnostic of 6 kcal. Table 2 gives the GB1 diagnostic for all the structures considered here. We see that all the stable adducts and four of the transition states have GB1 diagnostics greater than 6 kcal, so CCSD(T) and DLPNO-CCSD(T) may be less reliable for these cases. If we assumed that the benchmarks may be inaccurate by ~2 kcal and if we stipulate that a density functional calculation may be considered successful if the result is within ~1-2 kcal of the DLPNO-CCSD(T) value, we would arrive at a criterion that a density functional calculation can be considered successful if the deviation from DLPNO-CCSD(T) is less than ~3-4 kcal. Next, however, we must consider the deviation of DLPNO-CCSD(T) from CCSD(T). Our previous estimates of the reliability of DLPNO-CCSD(T) were based on tests from small molecules,[93] but more recent work[94] has shown that the errors may be much larger for the large molecules such as those involved in the present study.

We therefore tested the convergence of the DLPNO-CCSD(T) calculations with respect to the numerical parameters of the DLPNO part. To carry out this test, we considered reactants (**1**, **7**) and two important transition states **TS8** and **TS9**. We changed the cut off parameters and MP2 treatment and calculated the barrier heights; the results are in Table 3. This table shows that the NormalPNO

settings used for the benchmarks of the current work (which come from Refs. 6 and 7), give barrier heights differing from the TightPNO settings by 0.4 and 0.6 kcal for **TS8** and**TS9**, respectively. Based on these tests, we now increased the estimated unreliability of the DLPNO-CCSD(T) benchmarks to 2.5±1 kcal, and we arrive at a new criterion that a density functional calculation can be considered successful if the deviation from DLPNO-CCSD(T) is less than 4 kcal.

Results and discussion

A broad view. The present work considers 45 density functionals listed in Table 1; these provide a broad representation of the most used types of functionals. In some cases, molecular mechanics terms such as the D[43], D3, D3(BJ)[50,55,82], SAM[57] (used in APF-D), and ωB97X-D[72] models, were added. To allow a meaningful comparison with the benchmark values of ref 6, the calculations were all carried out using the optimized structures obtained by ωB97X-D/def2-TZVP, as retrieved from refs 6 and 7. All energies are given on molar basis. Before looking at the results in detail, we define four broad mean unsigned deviations (MADs) from the benchmark results, as given in Table 1:

B-B: Each reaction path has five barriers, yielding 5×4/2=10 pairs of barriers. For each pair of barriers, we compute the signed difference in their energies, and we compare it to the benchmark result. Since there are 3 reactions, this gives 30 data points, and the unsigned deviations yield MAD(B-B).

B-R: Here we consider the energies of the transition states relative to energies of the reactants (**1**+**7**). Each reaction has five transition states; this gives 15 data points, for which we compute the MAD from the benchmarks.

S-R: Here we consider the energies of the stable adducts relative to energies of the reactants. Each reaction has two stable intermediates and three products, which give 15 data points, for which we compute the MAD from the benchmarks.

B-S-R: Here we compute the MAD over all 60 data points.

The bottom row of Table 1 averages the MADs over the 45 functionals. We see average MADs of 7.3 kcal when we compare barriers to other barriers, 7.7 kcal when we compare barriers to separated reactants, and 12.7 kcal when we compare stable adducts to reactants. The largeness of these values confirms that the steps of this mechanism provide a difficult test.

Based on the considerations above we can judge a functional as reasonably successful if the MAD(B-S-R) is below 4 kcal. Table 1 shows that none of the 12 nonhybrid functionals passes this test, and none of the 12 global hybrids with less than 44% Hartree-Fock exchange passes the test.

However, 10 of the remaining 21 functionals have MAD(B-S-R) ≤ 4.0 kcal, and three have MAD(B-S-R) < 2.0 kcal: M05-2X-D3 (1.5 kcal), ωB97M-V (1.7), and M11 (2.7). These functionals all contain kinetic energy density and medium-to-high Hartree-Fock exchange, but Table 1 shows that not all functionals with kinetic energy density or high Hartree-Fock exchange perform well.

We find that molecular mechanics dispersion corrections significantly improve functionals with BLYP ingredients (BLYP, B3LYP, CAM-B3LYP, B2PLYP), but they lead to only small improvement or even decrease the accuracy for functionals with PBE ingredients (PBE, PBE-QIDH).

Close examination of Table 1, as summarized in the last two rows of Table 1, reveals that nonhybrid functionals have a different trend than hybrid functionals. Nonhybrid functionals are more accurate for barrier-to-separated-reactant comparisons (MAD: 8.9 kcal) than for barrier-to-barrier comparisons (11.4 kcal), whereas hybrid and doubly hybrid functionals show the reverse behavior (MADs of respectively 7.3 and 5.8 kcal).

Among all six classes of functionals, the accuracy is greater for barriers than for stable species (i.e.; MAD(B-R) < MAD(S-R)). This finding may at first seem surprising because one might expect barriers to be less accurate because of the difficulty of handling the partial bonds of transition states. However, the finding can be rationalized by considering Table 2, which present GB1 diagnostics for the formation of intermediates and transition states from reactants. This table shows that the stable species in the present mechanism tend to have higher GB1 diagnostics than the transition states. High GB1 diagnostics are an indication of multireference character[67,91] because Hartree-Fock exchange (present in B1LYP but not in BLYP) introduces static correlation error,[95,96] and multireference molecules are harder to treat for all functionals because Kohn-Sham DFT uses a single Slater determinant as the reference wave function.[76,97,98]

The quantity most important for sorting out the mechanisms would be MAD(B-B). It is understandable that, for the better-performing functionals, the B-B errors tend to be smaller than the errors for comparing transition states and adducts to reactants because the latter kind of comparison involves bringing bimolecular species together, which increases the number of atomic interactions, whereas the barrier-to-barrier comparisons are more like isomerizations. Seven of the 45 functionals get MAD(B-B) of 3.0 kcal or less and would therefore be most useful for sorting out mechanisms; conversely, 26 functionals have MAD(B-B) values ≥6.0 kcal and could easily predict misleading chemistry.

For **TS8** and **TS9**, the deviations from the benchmark are strongly correlated (Figure **S1**); however, there is not a good correlation of either of these with **TS6**. This explains why our previous

study, which considered only **TS8** and **TS9**, found smaller errors when comparing barriers to barriers than does the present study, where the B-B column of Table 1 includes all barrier-to-barrier comparisons; therefore, it is useful to look at additional comparisons in species-specific detail.

The need to use a good basis set for quantitative results was also highlighted by a specific analysis (see Supporting Information).

A closer look. We define MAD-T as the average of MAD(B-R) and MAD(S-R). Figure 2 reports the breakdown of MAD-T into the contribution of each of the three mechanisms (**1**, **1a**, and 1**b**). Although the methoxy-substitute case (**1b**) usually has largest errors, we see that all three reactions have similar deviations from the benchmarks. Therefore, in the following discussion we will mostly concentrate on the unsubstituted case.

Next consider the relative stability of final products (**11** and **12**) with respect to the reactants (**1**+**7**). Figure 3 shows that these relative energies span a large range from +18 to −46 kcal. While the general trend is close to that already discussed for the global MADs, it is striking that BLYP, B3LYP, and B1LYP incorrectly predict that the products are less stable than reactants. This is attributed to a poor treatment of intramolecular noncovalent interactions in large organic species that was first recognized in reactions involving the loss of a large ligand,[99] and clearly the same considerations apply to cycloadditions and cycloreversions. More specifically, this error originates from a poor treatment of the medium-range correlation energy.[99-105] It is ameliorated in PBE-D3 and B3LYP-D3 by adding an empirical molecular mechanics term to the functional, even though such corrections were nominally added to improve long-range correlation (rather than medium-range correlation). It is clear that only functionals that treat noncovalent interactions accurately can be successful for organic reactions of large molecules, even when the reactions involve changes in covalent bonding, not just changes in noncovalent interactions.

In most cases, the cycloaddition steps are correctly predicted to be exoergic, but insufficiently so (i.e., the bars in Figure 3 end to the right of the benchmark line); inaccuracies in medium-range correlation energy may again play a role here.

Figure 3 shows that, as a group, the local meta functionals do better than the gradient approximations. This is an example of the finding, known from previous work, that adding kinetic energy density as an ingredient in the functional (which is the extra ingredient in local meta functionals as compared to gradient approximations) allows for a better treatment of medium-range correlation energy, but it is insufficient in nonhybrid functionals. Figure 3 shows that some of the doubly hybrid functionals (those including LYP correlation) also underestimate the magnitude of the cycloaddition reaction energy. The inclusion of nonlocal correlation in these functionals was

partly motivated by the goal of improving long-range correlation, but this does not necessarily make the medium-range correlation energy accurate.

Although Figure 3 includes only **11** and **12**, Figure S2 shows that a similar behavior is observed for the relative stabilities of the other three stable species.

The energy differences between **TS5** and **TS6** or **TS7** determine the first bifurcation of the reaction path. Figure 4 shows these energy differences for the unsubstituted reaction, and Figures S3 and S4 show them for the substituted cases. We will discuss Figure 4. Several functionals agree with the benchmark data for **TS5** minus **TS7** within ~1 kcal, but the agreement is worse for **TS5** minus **TS6**, and in most cases the functionals that are accurate to ~1 kcal for one barrier perform rather poorly for the other. Four functionals get the sign wrong for **TS5** minus **TS6**, and two other functionals get the sign wrong for **TS5** minus **TS7**. The molecular mechanics terms have only a small effect here, in clear contrast with the behavior observed for the cycloaddition energies.

Figures 5, S5, and S6 compare the energy of **TS6** to that of **TS8**, leading to product **11** and to that of **TS9**, leading to product **12**. Again, the trends are similar for the three reactions, so we discuss only the unsubstituted case. The reaction is ambimodal if **TS6** lies above both **TS8** and **TS9**, as indicated by the benchmarks. Figure 5 shows that some of the density functionals predict **TS6** to be below **TS8**, and most of them predict **TS6** to be below **TS9**. We conclude that, if we accept the CCSD(T) benchmark as accurate, most of the density functionals predict the wrong character of the reaction mechanism. The functionals with the best agreement with benchmarks in Figure 5 are M05-2X-D3, ωB97M-V, M11, M11plus, PBE-QDIDH, and PBE-QDIDH-D3(BJ). These functionals come from all three of the classes of hybrid and doubly hybrid functionals.

It would be of great interest to understand why some functionals are more accurate than others, but the best functionals come from different classes, and within a given class of functionals, some functionals perform very well and others very poorly. Therefore, we cannot give a universally valid answer based only on the ingredients in a given functional. The only general conclusion that can be drawn is that all functionals that perform reasonably well are either hybrid or doubly hybrid. However, the arrangement of the functionals in Table 1 and in the figures makes it clear that the accuracy does not correlate simply with the percentage of Hartree-Fock exchange.

A possible explanation for some of the trends can be found by looking with chemist's eyes to the structures of the reaction intermediates. As mentioned before, the structures display a different number of double bonds, which in turn suggests a different degree of electronic delocalization. Delocalization error (DE), that is the unphysical overdelocalization of electronic distributions[106], is a common weakness arising from the approximate nature of the exchange-correlation functionals.

It could then be expected that the DE should be approximately constant along a reaction step connecting species with the same number of double bonds (**9** to **8**), while this error should be more significant when the number of double bonds changes (**9** to **12** and **8** to **11**). A qualitative measure of the DE associated with a given functional can be obtained by computing the difference between the ionization potential of a single He atom and that of a cluster composed of several well-separated He atoms (He-He distance equal to 10 Å)[107,108]. In Figure 6 the errors on the **TS6**, **TS8**, and **TS9** energies are reported as a function of the DE values computed for selected functionals. The energy error for **TS6** does not significantly depend on DE. However, for **TS8** and **TS9** the energies display clear qualitative correlations with the DE error, with a slope that depends on the functional family considered.

Concluding remarks

Our results for the cycloaddition mechanism under study show that many density functionals lead to seriously large errors and moreover differ from one another in predicting whether the reaction is ambimodal. Although the present study cannot be considered as a comprehensive benchmark, it does lead to some general conclusions on the application of density functional theory for chemical reactivity. First, only a small subset of the available functionals can provide a balanced description of complex and multifaceted reactions. The functionals that perform best have different ingredients and were obtained using different criteria and theoretical arguments, so one should not generalize one's expectations based solely on ingredients. The treatment of medium-range correlation energy, the reduction of the delocalization error, and the inclusion of Hartree-Fock exchange are clearly important, but these considerations, by themselves, do not enable one to see which functionals will have acceptable accuracy for a given complex mechanism. Thus, there is a clear need for more benchmarks on complex reaction mechanisms of large molecules. A bottleneck to such benchmarking is the general absence of converged quantum mechanical results for such problems. It must be realized that the field of organic chemistry applications may be a much more complex playground than is provided by reactions for which accurate benchmarks are available.

Computational details

The DFT calculations were done with Gaussian 16[109] a locally revised version of Gaussian 16,[110] and a development version of Gaussian[111], using the default computational thresholds. All spin states are singlets and were calculated with all orbitals doubly occupied. The results were

obtained with the aug-cc-pVTZ[112] basis set except for the section of the SI where we discuss the comparison to results obtained with the ma-QZVP[113] and 6-31G(d,p)[114] basis sets.

The DLPNO-CCSD(T) calculations were carried out with the ORCA program. Details concerning DLPNO-CCSD(T) calculations settings are reported in Table 3.[115,116]

The DFT and DLPNO-CCSD(T) energies were computed using the reference geometries reported in the work of Jamieson et al., considering also the subsequent erratum[6,7].

Acknowledgments

Pragya Verma contributed to the development and implementation of the M11plus functional. H.L. acknowledges financial support from the China Scholarship Council (grant no. 201908310062). This work was also supported in part by the U. S. Department of Energy through grant nos. DE-FG02-17ER16362, DE-SC0023383, and DE-SC0015997. Funded by the European Union (ERC, project MaMa, n. 101097351). Views and opinions expressed are however those of the author(s) only and do not necessarily reflect those of the European Union or the European Research Council Executive Agency. Neither the European Union nor the granting authority can be held responsible for them.

Supporting information

Tables and plots containing all calculated relative energies, basis set checks, diagnostics of multireference character, correlation of deviations from benchmark, and additional mean unsigned deviations from the benchmarks

References

1. Nørskov, J. K.; Abild-Pedersen, F.; Studt, F.; Bligaard, T. Density Functional Theory in Surface Chemistry and Catalysis. *Proc. Natl. Acad. Sci. U.S.A.* **2011**, *108*, 937–943.
2. Himo, F.; Lovell, T.; Hilgraf, R.; Rostovtsev, V. V.; Noodleman, L.; Sharpless, K. B.; Fokin, V. V. Copper(I)-Catalyzed Synthesis of Azoles. DFT Study Predicts Unprecedented Reactivity and Intermediates. *J. Am. Chem. Soc.* **2005**, *127*, 210–216.
3. Rao, L.; Xu, X.; Adamo, C. Theoretical Investigation on the Role of the Central Carbon Atom and Close Protein Environment on the Nitrogen Reduction in Mo Nitrogenase. *ACS Catal.* **2016**, *6*, 1567–1577.
4. Itô, S.; Fujise, Y.; Sato, M. Structure Determination of 2-Methoxytropone–Cycloheptatriene Adducts by Mass Spectrometry. *Tetrahedron Lett.* **1969**, 691-694.
5. Singh, V. Periselective Reactions of Tropone: A Novel Tandem π6s+ π4s, π4s+ π2s Reaction with Cycloheptatriene and π4s+ π2s Cycloaddition with Cyclohexa-2,4-Dienone. *Indian J. Chem. B* **1995**, *34B*, 847−850.
6. Jamieson, C. S.; Sengupta, A.; Houk, K. N. Cycloadditions of Cyclopentadiene and Cycloheptatriene with Tropones: All *Endo*-[6+4] Cycloadditions Are Ambimodal. *J. Am. Chem. Soc.* **2021**, *143*, 3918–3926.
7. Jamieson, C. S.; Sengupta, A.; Houk, K. N. Correction to "Cycloadditions of Cyclopentadiene and Cycloheptatriene with Tropones: All *Endo*-[6+4] Cycloadditions Are Ambimodal." *J. Am. Chem. Soc.* **2023**, *145*, 9366–9366.
8. Valtazanos, P.; Ruedenberg, K. Bifurcations and Transition States. Theor. Chem. Acc. 1986, 69, 281-307.
9. Krauss, W. A.; DePristo, A. E. Reaction Dynamics on Bifurcating Potential Energy Surfaces. Theor. Chim. Acta 1986, 69, 309-322.
10. Taketsugu, T.; Tajima, N.; Hirao, K. Approaches to Bifurcating Reaction Path. J. Chem. Phys. 1996, 105, 1933-1939.
11. Taketsugu, T.; Yanai, T.; Hirao, K.; Gordon, M.S. Dynamic Reaction Path Study of $SiH_4 + F^- \rightarrow SiH_4F^-$ and the Berry Pseudorotation with Valley-Ridge Inflection. J. Mol. Struct. THEOCHEM 1998, 451, 163-177.
12. Quapp, W.; Hirsch, M.; Heidrich, D. Bifurcation of Reaction Pathways: The Set of Valley Ridge Inflection Points of a Simple Three-Dimensional Potential Energy Surface. Theor. Chem. Acc. 1998, 100, 285-299.
13. Bakken, V.; Danovich, D.; Shaik, S.; Schlegel, H. B. A Single Transition State Serves Two Mechanisms: An ab Initio Classical Trajectory Study of the Electron Transfer and Substitution Mechanisms in Reactions of Ketyl Radical Anions with Alkyl Halides. J. Am. Chem. Soc. 2001, 123, 130-134.
14. Caramella, P.; Quadrelli, P.; Toma, L. An Unexpected Bispericyclic Transition Structure Leading to 4+2 and 2+4 Cycloadducts in the Endo Dimerization of Cyclopentadiene. J. Am. Chem. Soc. 2002, 124, 1130–1131.

15. Singleton, D. A.; Hang, C.; Szymanski, M. J.; Greenwald, E. E. A New Form of Kinetic Isotope Effect. Dynamic Effects on Isotopic Selectivity and Regioselectivity. J. Am. Chem. Soc. 2003, 125, 1176-1177.

16. Singleton, D. A.; Hang, C.; Szymanski, M. J.; Mayer, M. P.; Leach, A. G.; Kuwata, K. T.; Chen, J. S.; Greer, A.; Foote, C. S.; Houk, K. N. Mechanism of Ene Reactions of Singlet Oxygen. A Two-Step No-Intermediate Mechanism. J. Am. Chem. Soc. 2003, 125, 1319-1328.

17. González-Lafont, À.; Moreno, M.; Lluch, J.M. Variational Transition State Theory as a Tool to Determine Kinetic Selectivity in Reactions Involving a Valley-Ridge Inflection Point. J. Am. Chem. Soc. 2004, 126, 13089-13084.

18. Lasorne, B.; Dive, G.; Desouter-Lecomte, M. Wave Packets in a Bifurcating Region of an Energy Landscape: Diels-Alder Dimerization of Cyclopentadiene. J. Chem. Phys. 2005, 122, 184304.

19. Ussing, B. R.; Hang, C.; Singleton, D.A. Dynamic Effects on the Periselectivity, Rate, Isotope Effects, and Mechanism of Cycloadditions of Ketenes with Cyclopentadiene. J. Am. Chem. Soc. 2006, 128, 7594-7607.

20. Ess, D. H.; Wheeler, S. E.; Iafe, R. G.; Xu, L.; Celebi-Olcum, N.; Houk, K. N. Bifurcations on Potential Energy Surfaces of Organic Reactions. Angew. Chem. Int. Ed. 2008, 47, 7592–7601.

21. Thomas, J. B.; Waas, J. R.; Harmata, M.; Singleton, D. A. Control Elements in Dynamically Determined Selectivity on a Bifurcating Surface. J. Am. Chem. Soc. 2008, 130, 14544-14555.

22. Wang, Z.; Hirschi, J. S.; Singleton, D. A. Recrossing and Dynamic Matching Effects on Selectivity in a Diels–Alder Reaction. Angew. Chem.pdf Int. Ed. 2009, 121, 9320-8323.c

23. Zheng, J.; Papajak, E.; Truhlar, D. G. Phase Space Prediction of Product Branching Ratios: Canonical Competitive Nonstatistical Model. J. Am. Chem. Soc. 2009, 131, 15754-15760.

24. Glowacki, D. R.; Liang, C. H.; Marsden, S. P.; Harvey, J. N.; Pilling, M. J. Alkene Hydroboration: Hot Intermediates That React While They are Cooling. J. Am. Chem. Soc. 2010, 132, 13621-13623.

25. Hong, Y.; Tantillo, D. A Potential Energy Surface Bifurcation in Terpene Biosynthesis. Nature Chem. 2009, 1, 384–389.

26. Harabuchi, Y.; Taketsugu, T. A Significant Role of the Totally Symmetric Valley-Ridge Inflection Point in the Bifurcating Reaction Pathway. Theor. Chem. Acc. 2011, 130, 305–315.

27. Black, K.; Liu, P.; Xu, L.; Doubleday, C.; Houk, K. N. Dynamics, Transition States, and Timing of Bond Formation in Diels–Alder Reactions. Proc. Natl. Acad. Sci. USA 2012, 109, 12860–12865.

28. Collins, P.; Carpenter, B.K.; Ezra, G.S.; Wiggins, S.; Nonstatistical Dynamics on Potentials Exhibiting Reaction Path Bifurcations and Valley-Ridge Inflection Points. J. Chem. Phys. 2013, 139, 154108.

29. Pham, H. V.; Houk, K. N. Diels-Alder reactions of Allene with Benzene and Butadiene: Concerted, Stepwise, and Ambimodal Transition States. J. Org. Chem. 2014, 79, 8968-8976.

30. Rehbein, J.; Wulff, B. Chemistry in Motion – Off the MEP. Tetrahedron Lett. 2015, 56, 6931–6943.

31. Yu. P.; Chen, T. Q.; Yang, Z.; He, C. Q.; Patel, A.; Lam, Y-H.; Liu, C-Y.; Houk, K. N. Mechanisms and Origins of Periselectivity of the Ambimodal [6 + 4] Cycloadditions of Tropone to Dimethylfulvene. J. Am. Chem. Soc. 2017, 139, 8251−8258.

32. Villar López, R.; Faza, O.N.; Silva López, C. Dynamic Effects Responsible for High Selectivity in a [3,3] Sigmatropic Rearrangement Featuring a Bispericyclic Transition State. J. Org. Chem. 2017, 82, 4758–4765.

33. Hare, S. R.; Tantillo, D. J. Post-Transition State Bifurcations Gain Momentum – Current State of the Field. Pure Appl. Chem. 2017, 89, 679-698.

34. Xue, X.-S.; Jamieson, C. S.; Garcia-Borràs, M.; Dong, X.; Yang, Z.; Houk, K. N. Ambimodal Trispericyclic Transition State and Dynamic Control of Periselectivity. J. Am. Chem. Soc. 2019, 141, 3, 1217–1221.

35. Lee, S.; Goodman, J.M. Rapid Route-Finding for Bifurcating Organic Reactions. J. Am. Chem. Soc. 2020, 142, 9210-9219.

36. Bharadwaz, P.; Maldonado-Domínguez, M.; Srnec, M. Bifurcating Reactions: Distribution of Products from Energy Distribution in a Shared Reactive Mode. Chem. Sci. 2021, 12, 12682–12694.

37. Tantillo, D.J. Dynamic Effects on Organic Reactivity—Pathways to (and from) Discomfort. J. Phys. Org. Chem. 2021, 34, e4202.

38. Houk K. N.; Xue X.-S.; Liu F.; Chen Y.; Chen X.; Jamieson C. Computations on Pericyclic Reactions Reveal the Richness of Ambimodal Transition States and Pericyclases. Israel J. Chem. 2022, 62, e202100071.

39. Mansoori Kermani, M.; Li, H.; Ottochian, A.; Crescenzi, O.; Janesko, B. G.; Scalmani, G.; Frisch, M. J.; Ciofini, I.; Adamo, C.; Truhlar, D. G. Barrier Heights for Diels-Alder Transition States Leading to Pentacyclic Adducts: A Benchmark Study of Crowded, Strained Transition States of Large Molecules, *J. Phys. Chem. Lett.* **2023**, *14*, 6522–6531.

40. Gill, P. M. W.; Johnson, B. G.; Pople, J. A.; Frisch, M. J. An Investigation of the Performance of a Hybrid of Hartree-Fock and Density Functional Theory, *Int. J. Quantum Chem.* **1992**, *44* (*Symp. 26*) 319–331.

41. Peverati, R.; Truhlar. D. G. Exchange–Correlation Functional with Good Accuracy for Both Structural and Energetic Properties while Depending Only on the Density and Its Gradient. *J. Chem. Theory Comput.* **2012**, *8*, 2310-2319.

42. Perdew, J. P.; Burke, K.; Ernzerhof, M. Generalized Gradient Approximation Made Simple. *Phys. Rev. Lett.* **1996**, *77*, 3865–3868.

43. Grimme, S.; Antony, J.; Ehrlich, S.; Krieg, H. A Consistent and Accurate Ab Initio Parametrization of Density Functional Dispersion Correction (DFT-D) for the 94 Elements H-Pu. *J. Chem. Phys.* **2010**, *132*, 154104.

44. Peverati, R.; Truhlar, D. G. An Improved and Broadly Accurate Local Approximation to the Exchange–Correlation Density Functional: The MN12-L Functional for Electronic Structure Calculations in Chemistry and Physics. *Phys. Chem. Chem. Phys.* **2012**, *14*, 13171.

45. Yu, H. S.; He, X.; Truhlar, D. G. MN15-L: A New Local Exchange-Correlation Functional for Kohn–Sham Density Functional Theory with Broad Accuracy for Atoms, Molecules, and Solids. *J. Chem. Theory Comput.* **2016**, *12*, 1280–1293.

46. Zhao, Y.; Truhlar, D. G. A New Local Density Functional for Main-Group Thermochemistry, Transition Metal Bonding, Thermochemical Kinetics, and Noncovalent Interactions. *J. Chem. Phys.***2006**, *12*5, 194101.

47. Peverati, R.; Truhlar, D. G. M11-L: A Local Density Functional That Provides Improved Accuracy for Electronic Structure Calculations in Chemistry and Physics. *J. Phys. Chem. Lett.* **2012**, *3*, 117–124.

48. Wang, Y.; Jin, X.; Yu, H. S.; Truhlar, D. G.; He, X. Revised M06-L Functional for Improved Accuracy on Chemical Reaction Barrier Heights, Noncovalent Interactions, and Solid-State Physics. *Proc. Natl. Acad. Sci. U.S.A.* **2017**, *114*, 8487–8492.

49. Tao, J. M.; Perdew, J. P.; Staroverov, V. N.; Scuseria, G. E. Climbing the Density Functional Ladder: Nonempirical Meta-Generalized Gradient Approximation Designed for Molecules and Solids. *Phys. Rev. Lett.* **2003**, *91*, 146401.

50. Grimme, S.; Mück-Lichtenfeld, C. Accurate Computation of Structures and Strain Energies of Cyclophanes with Modern DFT Methods. *Isr. J. Chem.* **2012**, *52*, 180–192.

51. Mardirossian, N.; Head-Gordon, M. Mapping the Genome of Meta-Generalized Gradient Approximation Density Functionals: The Search for B97M-V. *J. Chem. Phys.* **2015**, *142*, 074111.

52. Vydrov, O. A.; Van Voorhis, T. Nonlocal van der Waals Density Functional: The Simpler the Better. *J. Chem. Phys.* **2010**, *133*, 244103.

53. Boese, A. D.; Handy, N. C. New Exchange-Correlation Density Functionals: The Role of the Kinetic-Energy Density, *J. Chem. Phys.* **2002**, *116*, 9559-9569.

54. Stephens, P. J.; Devlin, F. J.; Chabalowski, C. F.; Frisch, M. J. Ab Initio Calculation of Vibrational Absorption and Circular Dichroism Spectra Using Density Functional Force Fields. *J. Phys. Chem.* **1994**, *98*, 11623–11627.

55. Grimme, S.; Ehrlich, S.; Goerigk, L. Effect of the Damping Function in Dispersion Corrected Density Functional Theory. *J. Comput. Chem.* **2011**, *32*, 1456-1465.

56. Xu.; X.; Goddard III, W. A. The X3LYP Extended Density Functional for Accurate Descriptions of Nonbond Interactions, Spin States, and Thermochemical Properties, *Proc. Natl. Acad. Sci.* **2004**, *101*, 2673-2677.

57. Austin, A.; Petersson, G.; Frisch, M. J.; Dobek, F. J.; Scalmani, G.; Throssell, K. A Density Functional with Spherical Atom Dispersion Terms, *J. Chem. Theory Comput*. **2012**, *8*, 4989-5007.

58. Adamo, C.; Barone, V. Toward Reliable Adiabatic Connection Models Free from Adjustable Parameters. *Chem. Phys. Lett.* **1997**, *274*, 242-250.

59. Adamo, C.; Barone, V. Toward Reliable Density Functional Methods without Adjustable Parameters: The PBE0 Model. *J. Chem. Phys.* **1999**, *110*, 6158–6170.

60. Zhao, Y.; Truhlar, D. G. The M06 Suite of Density Functionals for Main Group Thermochemistry, Thermochemical Kinetics, Noncovalent Interactions, Excited States, and Transition Elements: Two New Functionals and Systematic Testing of Four M06-Class Functionals and 12 Other Functionals. *Theor. Chem Acc.* **2008***, 120*, 215–241.

61. Zhao, Y.; Truhlar, D. G. Design of Density Functionals that are Broadly Accurate for Thermochemistry, Thermochemical Kinetics, and Nonbonded Interaction, *J. Phys. Chem. A* **2005**, *109*, 5656-5667.

62. Peverati, R.; Truhlar. D. G. Communication: A Global Hybrid Generalized Gradient Approximation to the Exchange-Correlation Functional that Satisfies the Second-Order Density-Gradient Constraint and Has Broad Applicability in Chemistry. *J. Chem. Phys.* **2011**, *135*, 191102.

63. Wang, Y.; Verma, P.; Jin, X.; Truhlar, D. G.; He, X. Revised M06 Density Functional for Main-Group and Transition-Metal Chemistry. *Proc. Natl. Acad. Sci. U.S.A.* **2018**, *115*, 10257–10262.

64. Yu, H. S.; He, X.; Li, S. L.; Truhlar, D. G. MN15: A Kohn–Sham Global-Hybrid Exchange–Correlation Density Functional with Broad Accuracy for Multi-Reference and Single-Reference Systems and Noncovalent Interactions. *Chem. Sci.* **2016**, *7*, 5032–5051.

65. Liu, Y.; Zhang, C.; Liu, Z.; Truhlar, D. G.; Wang, Y.; He, X. Supervised Learning of a Chemistry Functional with Damped Dispersion. *Nat. Comput. Sci.* **2023**, *3*, 48−58.

66. Becke, A. D. A New Mixing of Hartree-Fock and Local Density-Functional Theories, *J. Chem. Phys.* **1993**, *98*, 1372-1377.

67. Zhao, Y.; Schultz, N. E.; Truhlar, D. G. Design of Density Functionals by Combining the Method of Constraint Satisfaction with Parametrization for Thermochemistry, Thermochemical Kinetics, and Noncovalent Interactions. *J. Chem. Theory Comput.* **2006**, *2*, 364-382.

68. Zhao, Y.; Truhlar, D. G. Density Functional for Spectroscopy: No Long-Range Self-Interaction Error, Good Performance for Rydberg and Charge-Transfer States, and Better Performance on Average than B3LYP for Ground States. *J. Phys. Chem. A* **2006**, *110*, 13126–13130.

69. Mardirossian, N.; Head-Gordon, M. ωB97M-V: A Combinatorially Optimized, Range-Separated Hybrid, Meta-GGA Density Functional with VV10 Nonlocal Correlation. *J. Chem. Phys.* **2016**, *144*, 214110.

70. Mardirossian, N.; Head-Gordon, M. ωB97X-V: A 10-Parameter, Range-Separated Hybrid, Generalized Gradient Approximation Density Functional with Nonlocal Correlation, Designed by a Survival-of-the-Fittest Strategy. *Phys. Chem. Chem. Phys.* **2014**, *16*, 9904-9924.

71. Yanai, T.; Tew, D. P.; Handy, N. C. A New Hybrid Exchange–Correlation Functional Using the Coulomb-Attenuating Method (CAM-B3LYP). *Chem. Phys. Lett.***2004**, *393*, 51–57.

72. Chai, J.-D.; Head-Gordon, M. Long-Range Corrected Hybrid Density Functionals with Damped Atom–Atom Dispersion Corrections. *Phys. Chem. Chem. Phys.* **2008**, *10*, 6615-6620.

73. Krukau, A. V.; Vydrov, O. A.; Izmaylov, A. F.; Scuseria, G. E. Influence of the Exchange Screening Parameter on the Performance of Screened Hybrid Functionals. *J. Chem. Phys.* **2006**, *125*, 224106.

74. Peverati, R.; Truhlar. D. G. Screened-Exchange Density Functionals with Broad Accuracy for Chemistry and Solid-State Physics. *Phys. Chem. Chem. Phys.* **2012**, *14*, 16187.

75. Peverati, R.; Truhlar, D. G. Improving the Accuracy of Hybrid Meta-GGA Density Functionals by Range Separation. *J. Phys. Chem. Lett.* **2011**, *2*, 2810–2817.

76. Verma, P.; Janesko, B. G.; Wang, Y.; He, X.; Scalmani, G.; Frisch, M. J.; Truhlar, D. G. M11plus: A Range-Separated Hybrid Meta Functional with Both Local and Rung-3.5 Correlation Terms and High Across-the-Board Accuracy for Chemical Applications. *J. Chem. Theory Comput.* **2019**, *15*, 4804–4815.

77. Grimme, S. Semiempirical Hybrid Density Functional with Perturbative Second-Order Correlation. *J. Chem. Phys.* **2006**, *124*, 034108.

78. Schwabe, T.; Grimme, S. Towards Chemical Accuracy for the Thermodynamics of Large Molecules: New Hybrid Density Functionals Including Non-Local Correlation Effects. *Phys. Chem. Chem. Phys.* **2006**, *8*, 4398-4401.

79. Schwabe, T.; Grimme, S. Double-hybrid density functionals with long-range dispersion corrections: higher accuracy and extended applicability, *Phys. Chem. Chem. Phys.* **2007**, *9*, 3397-3406.

80. Kozuch, S.; Martin, J. M. L. DSD-PBEP86: In Search of the Best Double-Hybrid DFT with Spin-Component Scaled MP2 and Dispersion Corrections. *Phys. Chem. Chem. Phys.* **2011**, *13*, 20104.

81. Brémond, É.; Sancho-García, J. C.; Pérez-Jiménez, Á. J.; Adamo, C. Communication: Double-Hybrid Functionals from Adiabatic-Connection: The QIDH Model. *J. Chem. Phys.* **2014**, *141*, 031101.

82. Sancho-García, J. C.; Brémond, É.; Savarese, M.; Pérez-Jiménez, A. J.; Adamo, C. Partnering Dispersion Corrections with Modern Parameter-Free Double-Hybrid Density Functionals. *Phys. Chem. Chem. Phys*, **2017**, *19*, 13481-13487.

83. Goerigk, L.; Hansen, A.; Bauer, C.; Ehrlich, S.; Najibi, A.; Grimme, S. A Look at the Density Functional Theory Zoo with the Advanced GMTKN55 Database for General Main Group Thermochemistry, Kinetics and Noncovalent Interactions. *Phys. Chem. Chem. Phys.* **2017**, *19*, 32184–32215.

84. Karton, A. Can Density Functional Theory 'Cope' with Highly Fluxional Shapeshifting Molecules? *Chem. Phys.* **2021**, *540*, 111013.

85. Santra, G.; Calinsky, R.; Martin, J. M. L. Benefits of Range-Separated Hybrid and Double-Hybrid Functionals for a Large and Diverse Dataset of Reaction Energies and Barrier Heights. *J. Phys. Chem. A* **2022**, *126*, 5492-5505.

86. Janesko, B. G.; Verma, P.; Scalmani, G.; Frisch, M. J.; Truhlar, D. G. M11plus, a Range-Separated Hybrid Meta Functional Incorporating Nonlocal Rung-3.5 Correlation, Exhibits Broad Accuracy on Diverse Databases. *J. Phys. Chem. Lett.* **2020**, *11*, 3045–3050.

87. Mardirossian, N.; Head-Gordon, M. ωB97M-V: A Combinatorially Optimized, Range-Separated Hybrid, Meta-GGA Density Functional with VV10 Nonlocal Correlation. *J. Chem. Phys.* **2016**, *144*, 214110.

88. Riplinger, C.; Sandhoefer, B.; Hansen, A.; Neese, F. Natural Triple Excitations in Local Coupled Cluster Calculations with Pair Natural Orbitals. *J. Chem. Phys.* **2013**, *139*, 134101.

89. Raghavachari, K.; Trucks, G. W.; Pople, J. A.; Head-Gordon, M. A Fifth-Order Perturbation Comparison of Electron Correlation Theories. *Chem. Phys. Lett.* **1989**, *157*, 479−483.

90. Fogueri, U. R.; Kozuch, S.; Karton, A.; Martin, J. M. L. A Simple DFT-Based Diagnostic for Nondynamical Correlation, Th*eor. Chem. Acc.* **2013**, *132*, 1291.

91. Schultz, N. E.; Zhao, Y.; Truhlar, D. G. Density Functionals for Inorganometallic and Organometallic Chemistry. *J. Phys. Chem. A* **2005**, *109*, 11127−11143.

92. Zhao, Y.; Tishchenko, O.; Gour, J. R.; Li, W.; Lutz, J. J.; Piecuch, P.; Truhlar, D. G. Thermochemical Kinetics for Multireference Systems: Addition Reactions of Ozone. *J. Phys. Chem. A* **2009**, *113*, 5786−5799.

93. Liakos, D. G.; Sparta, M.; Kesharwani, M. K.; Martin, J. M. L.; Neese, F. Exploring the Accuracy Limits of Local Pair Natural Orbital Coupled-Cluster Theory. *J. Chem. Theory Comput.* **2015**, *11*, 1525− 1539.

94. Altun, A.; Ghosh, S.; Riplinger, C.; Neese, F.; Bistoni, G. Addressing the System-Size Dependence of the Local Approximation Error in Coupled-Cluster Calculations. *J. Phys. Chem. A* **2021**, *125*, 9932-9939.

95. Yu, H. S.; Li, S. L.; Truhlar, D. G. Perspective: Kohn-Sham Density Functional Theory Descending a Staircase. *J. Chem. Phys.* **2016**, *145*, 130901.

96. Zhang, D.; Truhlar, D. G. Unmasking Static Correlation Error in Hybrid Kohn−Sham Density Functional Theory. *J. Chem. Theory Comput.* **2020**, *16*, 5432−5440.

97. Yu, H. S.; Li, S.; Truhlar, D. G. Perspective: Kohn-Sham Density Functional Theory Descending a Staircase. *J. Chem. Phys.* **2016**, *145*, 130901.

98. Verma, P.; Wang, Y.; Ghosh, S.; He, X.; Truhlar, D. G. Revised M11 Exchange-Correlation Functional for Electronic Excitation Energies and Ground-State Properties. *J. Phys. Chem. A* **2019**, *123*, 2966−2990.

99. Zhao, Y.; Truhlar, D. G. Attractive Noncovalent Interactions in Grubbs Second-Generation Ru Catalysts for Olefin Metathesis. *Org. Lett.* **2007**, *9*, 1967-1970.

100. Zhao, Y.; Truhlar, D. G. A Density Functional Theory that Accounts for Medium-Range Correlation Energies in Organic Chemistry. *Org. Lett.* **2006**, *8*, 5753−5755.

101. Wodrich, M. D.; Corminboeuf, C.; Schreiner, P.R.; Fokin, A. A.; Von Schleyer, P. R.; How accurate are DFT treatments of organic energies? O*rg. Lett.* **2007**, *9*, 1851–1854.

102. Schreiner, P. R.; Relative energy computations with approximate density functional theory - A caveat! *Angew. Chem. Int. Ed.* **2008**, *46*, 4217–4219.

103. Zhao, Y.; Truhlar, D. G. Density Functionals with Broad Applicability in Chemistry. *Acc. Chem. Res.* **2008**, *41*, 157-167.

104. Plumley, J.A.; Evanseck, J. D. Hybrid Meta-Generalized Gradient Functional Modeling of Boron–Nitrogen Coordinate Covalent Bonds, *J. Chem. Theory Comput.* **2008**, *4*, 1249–1253.

105. Zhao, Y.; Truhlar, D. G. A Prototype for Graphene Material Simulation: Structures and Interaction Potentials of Coronene Dimers. *J. Phys. Chem. C* **2008**, *112*, 4061-4067.

106. Johnson, E. R.; Mori-Sánchez, P.; Cohen, A. J.; Yang, W. Delocalization Errors in Density Functionals and Implications for Main-Group Thermochemistry. *J. Chem. Phys.* **2008**, *129*, 204112.

107. Li, C.; Zheng, X.; Su, N. Q.; Yang, W. Localized Orbital Scaling Correction for Systematic Elimination of Delocalization Error in Density Functional Approximations. *National Science Rev.* **2018**, *5,* 203–215.

108. Bao, J. L.; Wang, Y.; He, X.; Gagliardi, L.; Truhlar, D. G. Multiconfiguration Pair-Density Functional Theory Is Free from Delocalization Error. *J. Phys. Chem. Lett.* **2017**, *8*, 5616–5620.

109. Gaussian 16, Revision C.01, Frisch, M. J.; Trucks, G. W.; Schlegel, H. B.; Scuseria, G. E.; Robb, M. A.; Cheeseman, J. R.; Scalmani, G.; Barone, V.; Petersson, G. A.; Nakatsuji, H.; Li, X.; Caricato, M.; Marenich, A. V.; Bloino, J.; Janesko, B. G.; Gomperts, R.; Mennucci, B.; Hratchian, H. P.; Ortiz, J. V.; Izmaylov, A. F.; Sonnenberg, J. L.; Williams-Young, D.; Ding, F.; Lipparini, F.; Egidi, F.; Goings, J.; Peng, B.; Petrone, A.; Henderson, T.; Ranasinghe, D.; Zakrzewski, V. G.; Gao, J.; Rega, N.; Zheng, G.; Liang, W.; Hada, M.; Ehara, M.; Toyota, K.; Fukuda, R.; Hasegawa, J.; Ishida, M.; Nakajima, T.; Honda, Y.; Kitao, O.; Nakai, H.; Vreven, T.; Throssell, K.; Montgomery, J. A., Jr.; Peralta, J. E.; Ogliaro, F.; Bearpark, M. J.; Heyd, J. J.; Brothers, E. N.; Kudin, K. N.; Staroverov, V. N.; Keith, T. A.; Kobayashi, R.; Normand, J.; Raghavachari, K.; Rendell, A. P.; Burant, J. C.; Iyengar, S. S.; Tomasi, J.; Cossi, M.; Millam, J. M.; Klene, M.; Adamo, C.; Cammi, R.; Ochterski, J. W.; Martin, R. L.; Morokuma, K.; Farkas, O.; Foresman, J. B.; Fox, D. J. Gaussian, Inc., Wallingford CT, 2016.

110. Kanchanakungwankul, S.; Zhang, D.; Truhlar, D. G. revG16; a modified version of Gaussian 16.

111. Gaussian GDV, Revision I.14+, Frisch, M. J.; Trucks, G. W.; Schlegel, H. B.; Scuseria, G. E.; Robb, M. A.; Cheeseman, J. R.; Scalmani, G.; Barone, V.; Petersson, G. A.; Nakatsuji, H.; Li, X.; Caricato, M.; Marenich, A. V.; Bloino, J.; Janesko, B. G.; Gomperts, R.; Mennucci, B.; Hratchian, H. P.; Ortiz, J. V.; Izmaylov, A. F.; Sonnenberg, J. L.; Williams-Young, D.; Ding, F.; Lipparini, F.; Egidi, F.; Goings, J.; Peng, B.; Petrone, A.; Henderson, T.; Ranasinghe, D.; Zakrzewski, V. G.; Gao, J.; Rega, N.; Zheng, G.; Liang, W.; Hada, M.; Ehara, M.; Toyota, K.; Fukuda, R.; Hasegawa, J.; Ishida, M.; Nakajima, T.; Honda, Y.; Kitao, O.; Nakai, H.; Vreven, T.; Throssell, K.; Montgomery, J. A., Jr.; Peralta, J. E.; Ogliaro, F.; Bearpark, M. J.; Heyd, J. J.; Brothers, E. N.; Kudin, K. N.; Staroverov, V. N.; Keith, T. A.; Kobayashi, R.; Normand, J.; Raghavachari, K.; Rendell, A. P.; Burant, J. C.; Iyengar, S. S.; Tomasi, J.; Cossi, M.; Millam, J. M.; Klene, M.; Adamo, C.; Cammi, R.; Ochterski, J. W.; Martin, R. L.; Morokuma, K.; Farkas, O.; Foresman, J. B.; Fox, D. J. Gaussian, Inc., Wallingford CT, 2023.

112. Kendall, R. A.; Dunning Jr.; T. H.; Harrison, R. J. Electron Affinities of the First-Row Atoms Revisited. Systematic Basis Sets and Wave Functions. *J. Chem. Phys.* **1992**, *96*, 6796−6806.

113. Zheng, J.; Xu, X.; Truhlar, D. G. Minimally Augmented Karlsruhe Basis Sets. *Theor. Chem. Acc.* **2011**, *128*, 295−305.

114. Hehre, W. J.; Ditchfield, R.; Pople, J. A. Self-Consistent Molecular-Orbital Methods 12. Further Extensions of Gaussian-Type Basis Sets for Use in Molecular-Orbital Studies of Organic-Molecules. *J. Chem. Phys.* **1972***, 56*, 2257−2261.

115. Neese, F. The ORCA Program System. *WIREs Comput. Mol. Sci.* **2012,** *2*, 73−78.

116. Neese, F. Software Update: The ORCA Program System, Version 4.0. *WIREs Comput. Mol. Sci.* **2018**, *8*, e1327.

Table 1. Exchange-Correlation Functionals Considered in this Work, Arranged According to the Percentage of Hartree–Fock Exchange at Short-Range[a] and Showing Four Key Measures of error

Functional	%HFX[b]	%PT2[b]	Reference	MAD (kcal) B-B	B-R	S-R	B-S-R
Gradient approximations							
BLYP	0	0	40	17.3	21.5	43.0	24.8
N12	0	0	41	8.9	7.2	20.7	11.4
PBE	0	0	42	9.5	6.2	19.7	11.2
PBE-D3	0	0	42,43	9.7	7.9	14.3	10.4
Local meta functionals							
MN12-L[c]	0	0	44	11.8	8.1	14.2	11.5
MN15-L[c]	0	0	45	9.6	7.0	9.5	8.9
M06-L[c]	0	0	46	13.8	9.5	18.4	13.9
M11-L[c]	0	0	47	10.6	7.0	15.2	10.9
revM06-L[c]	0	0	48	10.9	7.3	15.4	11.1
TPSS-D3(BJ)[c]	0	0	49,50	10.7	8.5	15.6	11.4
Functionals with density-based nonlocal correlation							
B97M-V[c]	0	0	51	10.8	7.8	12.7	10.5
VV10[d]	0	0	52	13.3	9.3	17.1	13.3
Global hybrid functionals							
τHCTHhyb[c]	13.265	0	53	8.8	8.7	20.1	11.6
B3LYP	20	0	54	12.0	18.6	30.7	18.3
B3LYP-D3	20	0	43,54	12.1	12.7	20.0	14.2
B3LYP-D3(BJ)	20	0	54,55	10.9	7.6	16.7	11.5
X3LYP	21.8	0	56	11.5	17.0	28.3	17.1
APF-D	22.945	0	57	5.0	6.5	1.8	4.6
B1LYP	25	0	58	11.7	20.4	30.9	18.7
PBE0	25	0	59	4.0	4.0	8.9	5.2
M06[c]	27	0	60	7.4	4.9	9.1	7.2
PW6B95-D3[c]	28	0	43,61	6.5	4.2	10.1	6.8
SOGGA11-X	40.15	0	62	4.0	8.4	8.8	6.3
revM06[c]	40.4	0	63	4.5	4.1	7.5	5.2
MN15[c]	44	0	64	4.0	2.4	3.8	3.5
CF22D[c]	46.2806	0	65	3.9	2.5	3.7	3.5
BHandHLYP	50	0	66	6.2	19.0	18.4	12.5
M06-2X[c]	54	0	60	3.0	2.5	4.5	3.2
M05-2X-D3[c]	56	0	43,67	1.3	0.8	2.6	1.5
M06-HF[c]	100	0	68	7.2	4.9	6.8	6.5
Range-separated hybrid functionals							
ωB97M-V[c]	15/100	0	69	2.1	1.4	1.4	1.7
ωB97X-V	16.7/100	0	70	4.2	2.8	6.2	4.3
CAM-B3LYP	19/65	0	71	5.1	14.6	15.6	10.1

ωB97X-D	22/100	0	72	3.3	2.7	2.9	3.0
HSE06[c,e]	25/0	0	73	5.5	4.7	11.1	6.7
MN12-SX[c]	25/0	0	74	8.1	5.6	11.7	8.4
N12-SX	25/0	0	74	4.2	3.8	8.5	5.1
M11[c]	42.8/100	0	75	1.2	4.8	3.6	2.7
M11plus[c]	42.8/100	0	76	2.9	4.6	2.4	3.2
Doubly hybrid functionals							
B2PLYP	53	27	77	8.5	6.7	17.8	10.4
B2PLYP-D3(BJ)	53	27	55,77	8.5	6.3	12.1	8.9
mPW2PLYP-D	55	25	78,79	7.0	13.1	9.2	9.1
DSD-PBEP86	69	22/52	80	3.0	6.6	0.6	3.3
PBE-QIDH	69.336	33.333	81	1.8	5.8	4.5	3.5
PBE-QIDH-D3(BJ)	69.336	33.333	81,82	1.7	8.4	6.6	4.6
Average – all 45				7.3	7.7	12.5	8.7
Average – 12 nonhybrid				11.4	8.9	18.0	12.4
Average – 33 hybrid and doubly hybrid				5.8	7.3	10.5	7.3

[a] When the percentage of HF exchange at short range is the same, the functionals are listed alphabetically.

[b] %HFX is the percentage of nonlocal Hartree-Fock exchange energy; %PT2 is the percentage of nonlocal second-order perturbation-theory correlation energy. When two numbers are given, the first is the limiting value at small interelectronic separation (r_{12}), and the second is the limiting value at large r_{12}.

[c] These functionals are meta, i.e.; they contain kinetic energy density.

[d] This is the original VV10 functional as indicated in reference 21, composed by the rPW86 exchange and the local PBE correlation plus the VV10 correlation.

[e]There are multiple versions of the HSE06 functional; we used the version given by the OHSE1PBE keyword in *Gaussian*.

Table 2 GB1 Diagnostics[a] for the Change in Multireference Character in the Reactions of Cycloheptatriene

Species	tropone	2-chlorotropone	2-methoxytropone
8	9	10	10
9	10	10	11
10	8	9	9
11	15	16	17
12	15	16	17
TS5	4	3	3
TS6	2	1	2
TS7	3	2	2
TS8	6	7	8
TS9	6	7	6

[a] $|\Delta E(\mathrm{BLYP}) - \Delta E(\mathrm{B1LYP})|$ in kcal for formation of the species or transition state from reactants (**1** and **7)**

Table 3 DLPNO-CCSD(T) threshold tests

	NormalPNO	TightPNO	TightPNO – NormalPNO
Setting names	**Settings used**		
$T_{CutPairs}$[a]	10^{-4}	10^{-5}	
T_{CutDO}[b]	1×10^{-2}	5×10^{-3}	
T_{CutPNO}[c]	3.33×10^{-7}	1.00×10^{-7}	
T_{CutMKN}[d]	10^{-3}	10^{-3}	
MP2 pair treatment	semicanonical	full iterative	
Species	**Relative energies (kcal)**		
1+7	0.00	0.00	
TS8	9.03	9.41	0.38
TS9	14.43	15.02	0.59

[a]cut-off for the PNO truncation (controls the number of PNOs per electron pair)
[b]cut-off for the DLPNO domain construction
[c]cut-off for the pair truncation (controls a perturbative selection of significant pairs)
[d]cut-off for the local fit (controls the size of the fit set for each electron pair)
[e]For each column, energies are relative to **1**+**7** for the settings of that column.

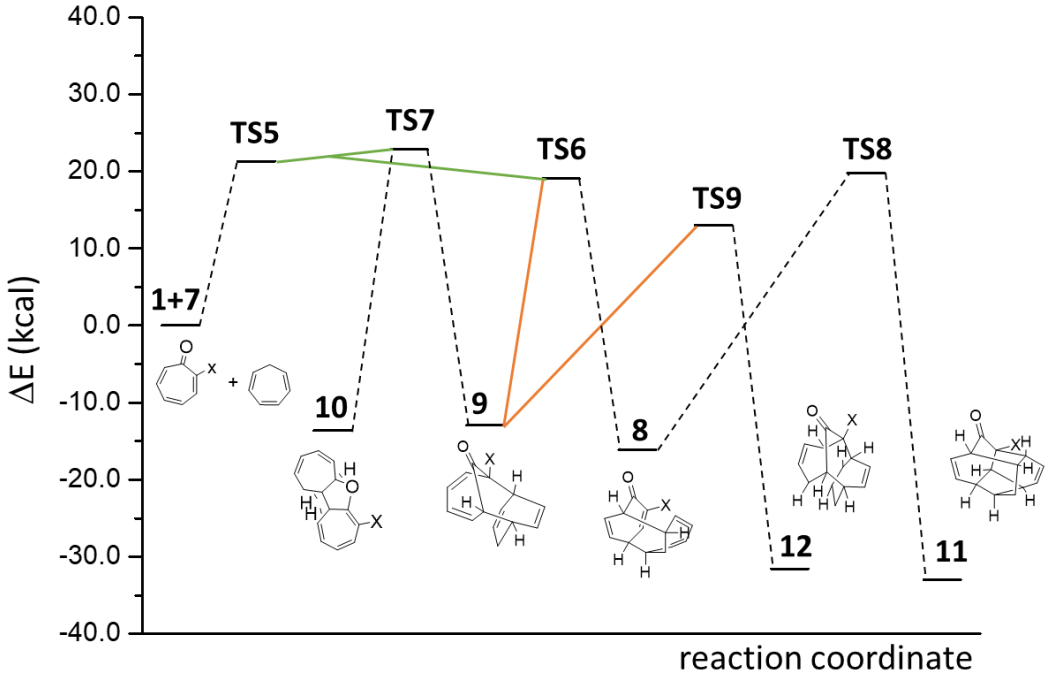

Figure 1. Energy profile for the unsubstituted reaction, including the sketches of the reactants, intermediates, and products. The energies shown are the DLPNO-CCSD(T)/cc-pVQZ calculations of Refs. 6 and 7.

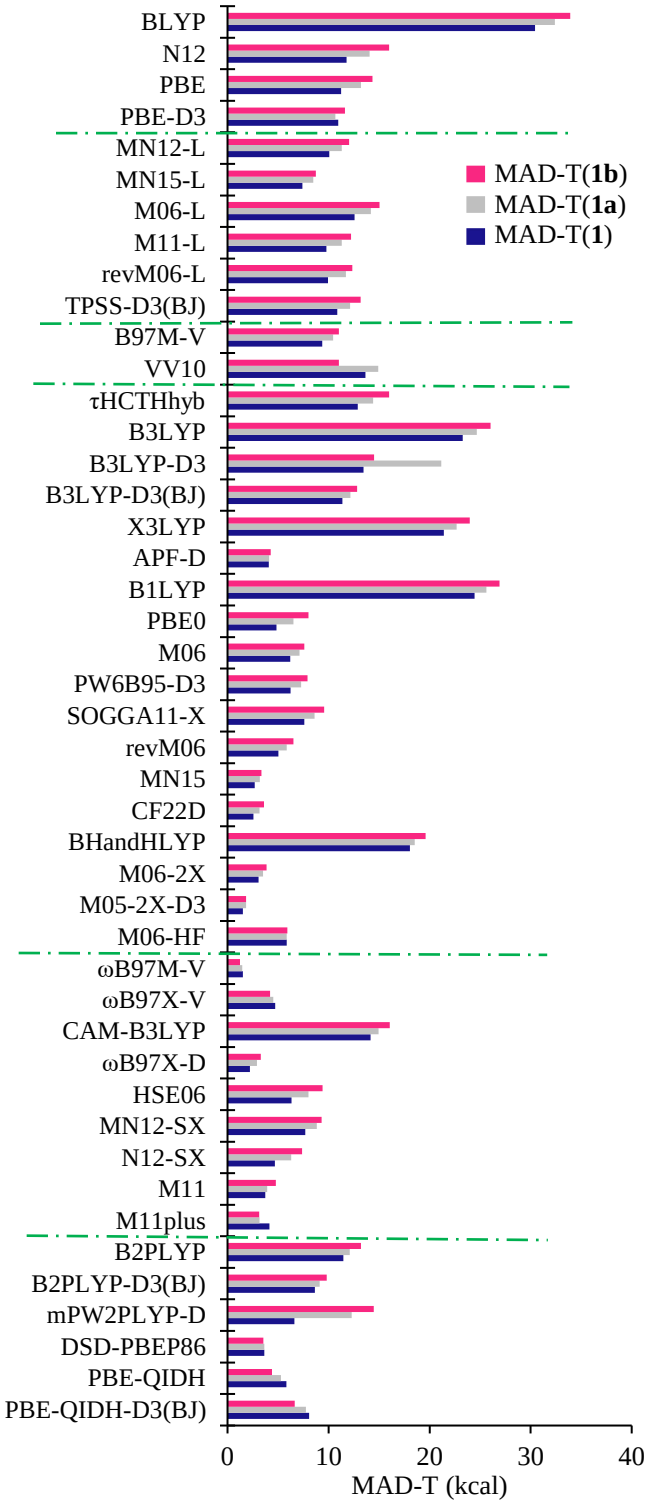

Figure 2. MAD-T for the three reactions. The dot-dash horizontal lines separate the classes of functionals as organized in Table 1.

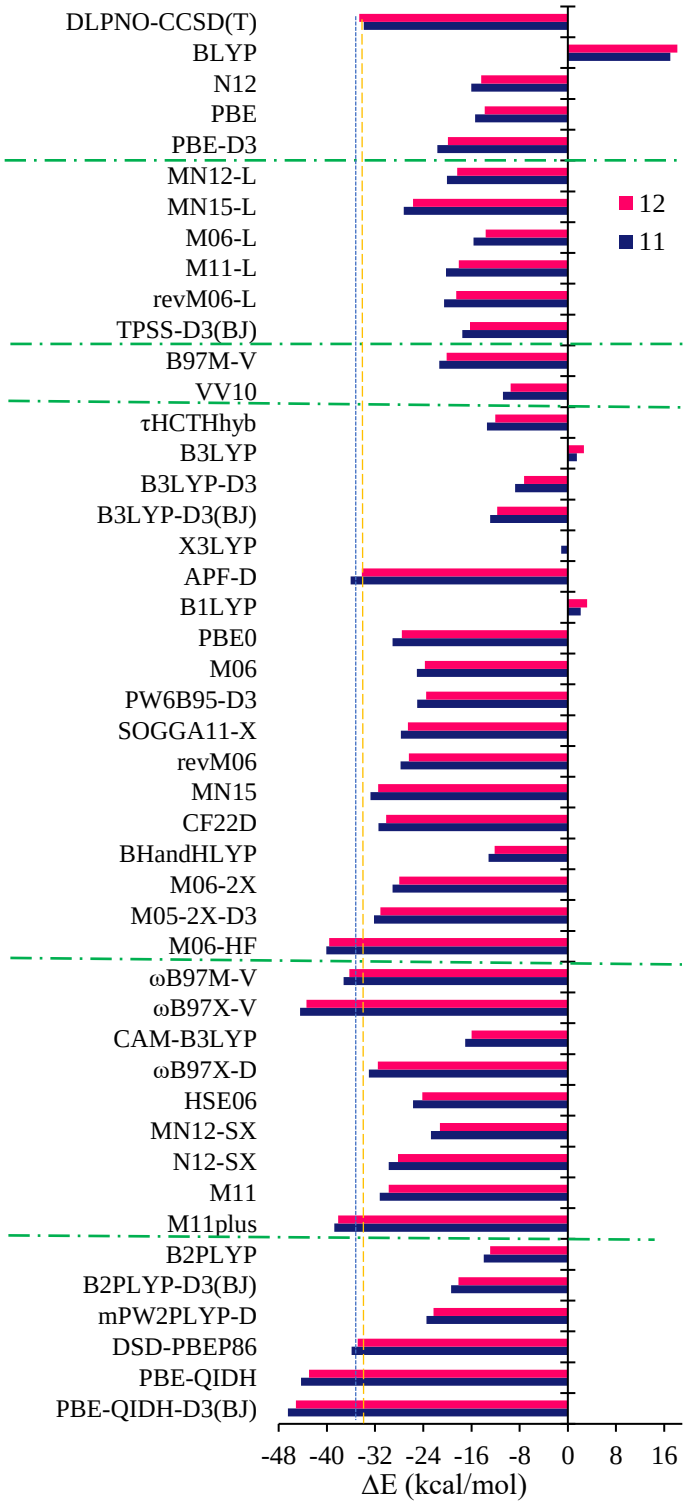

Figure 3. Relative energies (kcal) of products **11** and **12** with respect to the reactants **1+7**. The vertical lines guide the eye for comparison to the benchmark result at the top. The horizontal lines separate the classes of functionals in Table 1.

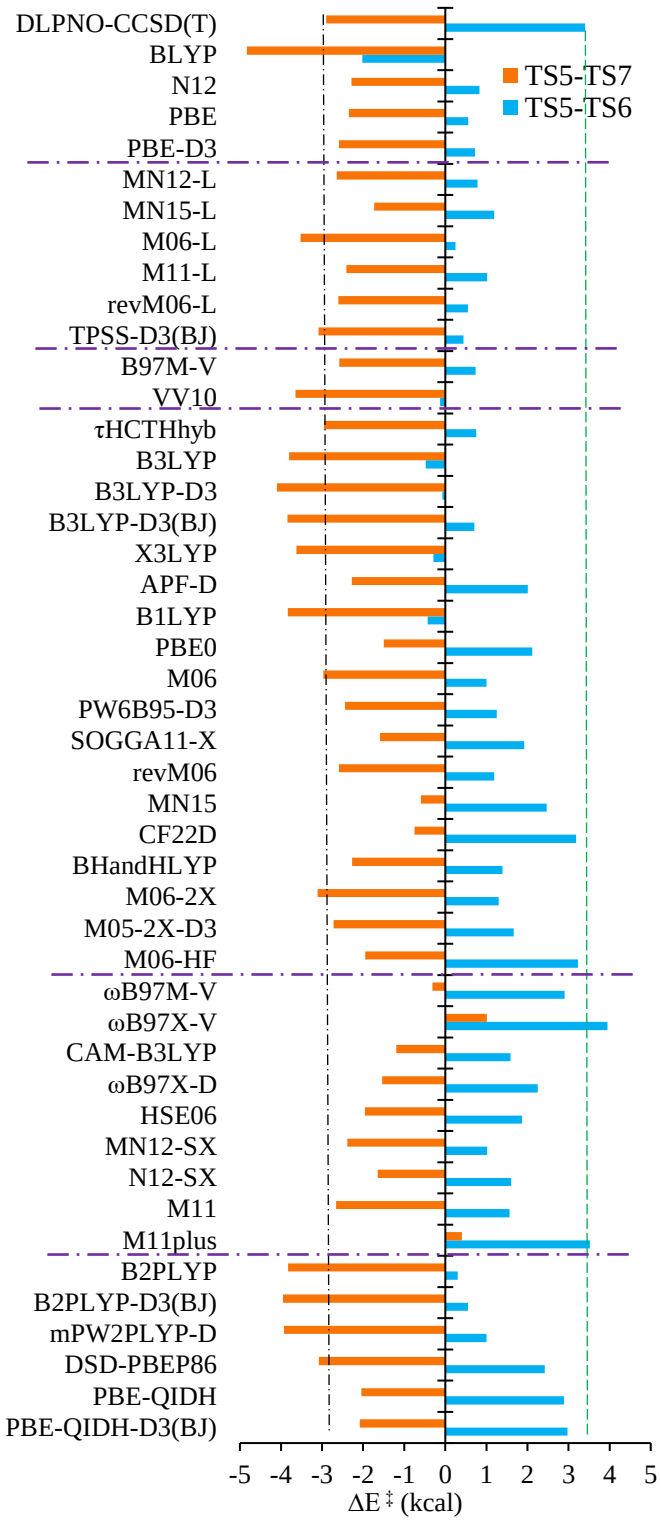

Figure 4. Energy differences ($\Delta E^{\ddagger}$, kcal) between **TS5** and **TS6** or **TS7** for unsubstituted tropone. Positive values indicate that **TS5** is higher than **TS6** or **TS7**, and negative values the opposite. The dot-dash horizontal lines separate the classes of functionals as organized in Table 1. The vertical lines are to guide the eye for comparison to the benchmarks.

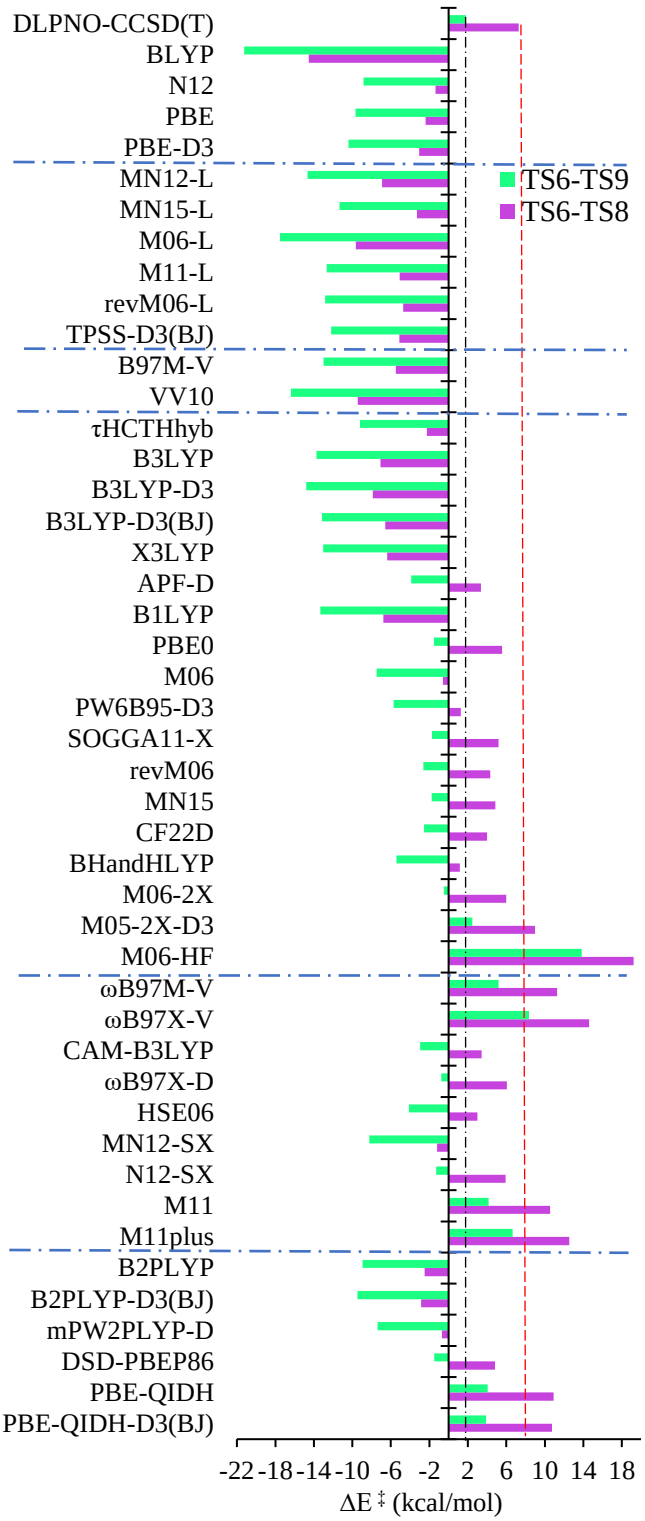

Figure 5. Energy differences (ΔE ‡, kcal) between **TS6** and **TS8** or **TS9** for unsubstituted tropone. Positive values indicate that TS6 is higher than TS8 or TS9, and negative values the opposite. The dot-dash horizontal lines separate the classes of functionals as organized in Table 1. The vertical lines are to guide the eye for comparison to the benchmarks.

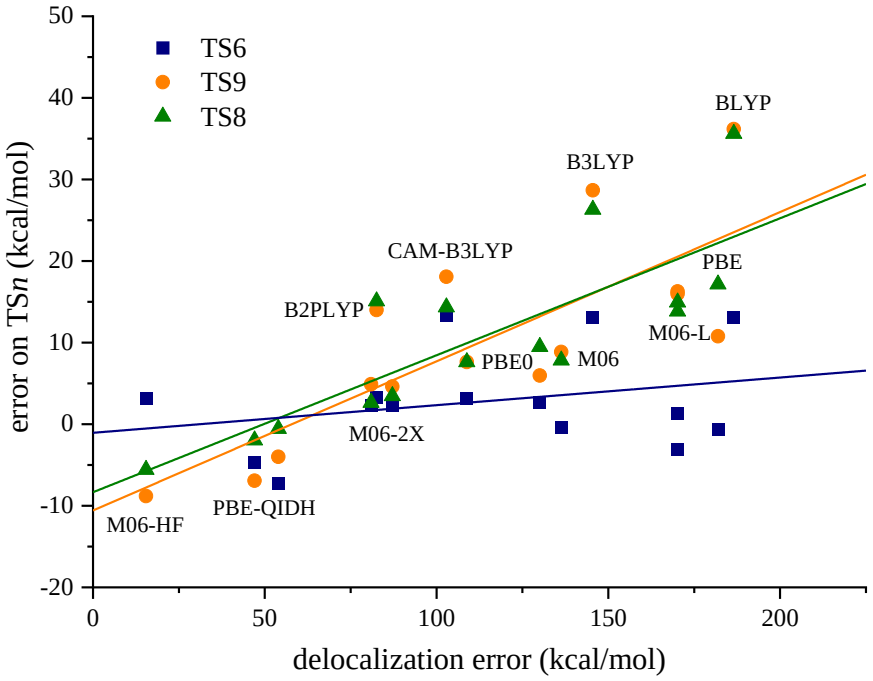

Figure 6. Computed error on **TS6**, **TS9** and **TS8** (error on TS*n*, kcal) as a function of the delocalization error. Some functionals are explicitly indicated for **TS8**. The continuous line corresponds to linear fitting on all the points for a given TS*n*.

TOC